Supporting information

Ultrathin Fe-NiO nanosheets as catalytic charge reservoir for planar Mo-doped $BiVO_4$ photoanode

Lei Li,[a,b] Xiaogang Yang,*[a,b,c] Yan Lei,[a,c] Haili Yu,[a,d] Zhongzheng Yang,[a,b] Zhi Zheng*[a,c] and Dunwei Wang[e]

a. Key Laboratory for Micro-Nano Energy Storage and Conversion Materials of Henan Province, College of Advanced Materials and Energy, Institute of Surface Micro and Nanomaterials, Xuchang University, Xuchang, Henan 461000, China.
b. Henan Key Material Laboratory, North China University of Water Resources and Electric Power, Zhengzhou, Henan, 450053, China.
c. Henan Joint International Research Laboratory of Nanomaterials for Energy and Catalysis, Xuchang University, Xuchang, Henan 461000, China.
d. College of Chemistry and Molecular Engineering, Zhengzhou University, Zhengzhou, Henan, 450001, China
e. Department of Chemistry, Merkert Chemistry Center, Boston College, 2609 Beacon St., Chestnut Hill, MA 02467 USA

*Corresponding address: E-mail: xiaogang.yang@gmail.com (X.Y.) and zzheng@xcu.edu.cn (Z.Z.)

Theoretical simulation.

Suppose only two reactions contributes to the transient charge phenomena. In addition, there are two assumptions: a) ultrafast charge excitation caused by laser (~ps), b) the bulk charge recombination (~ps). This resulted in an apparent steady state of excited but unseparated charge densities, such as the excited charge densities ($Q_{exc,0}$). Since the band bending under dark conditions causes an internal built-in field that will drive the excited charge to the solid/air surface. The possible charge reactions will follow the process:

$$Q_{exc} \xrightarrow{k_{sep}} Q_{sep} \xrightarrow{k_{rec}} Q_{rec} \qquad (1)$$

where the $Q_{exc,}$ Q_{sep} and Q_{rec} represent the excited unseparated charge density, separated but not recombined charge density (only this one can be detected by TSPV), the recombined charge densities (cannot be detected, as it is "dead" one), respectively.

For simplification, $Q_{exc,0}$ is the initial excited charge density just after the laser pulse; during the above serial charge reactions, the bulk recombination reactions still exist, but we combine it into the apparent recombination rates (k_{rec}).

Then the reactions can be displayed as follows, with the boundary conditions (t=0 and t=t):

	$Q_{exc} \xrightarrow{k_{sep}}$	$Q_{sep} \xrightarrow{k_{rec}}$	Q_{rec}
$t=0$	$Q_{exc,0}$	0	0
t=t	Q_{exc}	Q_{sep}	Q_{rec}

Since the Q_{sep} and Q_{rec} do not exist from the beginning, then the kinetic reactions can be written as:

$$\begin{cases} \dfrac{d\left(Q_{exc}\right)}{dt} = -k_{sep}Q_{exc} & (2a) \\ \dfrac{d\left(Q_{sep}\right)}{dt} = k_{sep}Q_{exc} - k_{rec}Q_{sep} & (2b) \\ \dfrac{d\left(Q_{rec}\right)}{dt} = k_{rec}Q_{sep} & (2c) \end{cases}$$

where Eq. 2a stands for the charge separation causes the initial excited charge density

decrease; Eq. 2b stands for the separated charges from the excited one (production) and consumption; Eq. 2c stands for the consumption of the separated charge by surface recombination.

By a similar treatment on this-serial chemical reactions in general physical chemistry, the function of the t_{max} and Q_{sep} can be obtained.

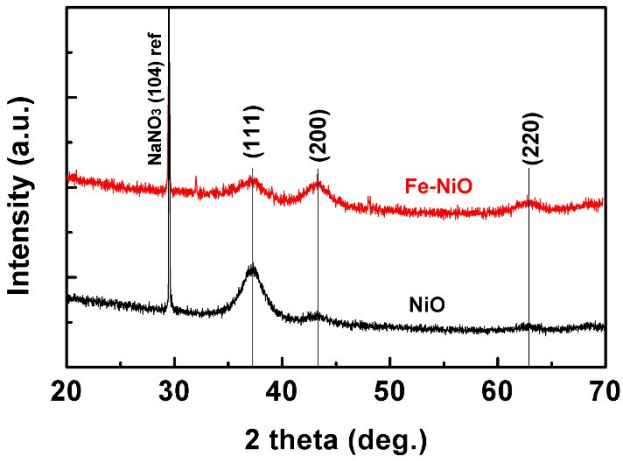

Figure S1. XRD of NiO (black curve) and Fe-doped NiO (red curve) nanosheets. The diffraction peak at ~29.5° corresponded to the (104) distance of $NaNO_3$, which was used as reference for angle calibration.

The XRD peak of Fe-doped NiO slightly shifted to lower angle, possibly due to the high lattice stress. The strong (111) peak of NiO indicated a higher orientation of the nanosheets than the Fe-doped one.

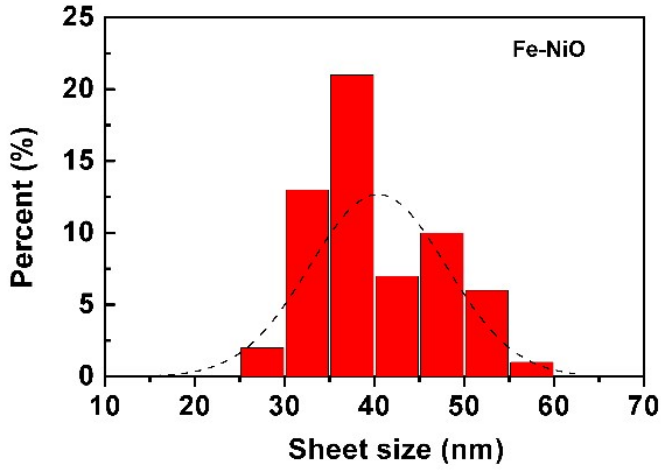

Figure S2. Size distribution of the Fe-doped NiO nanosheets.

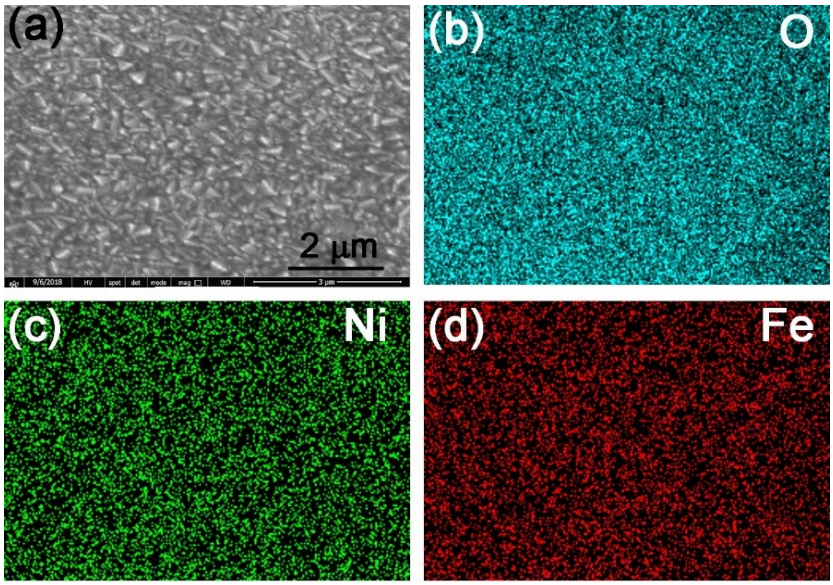

Figure S3. SEM image (a) and EDX mapping images of the Fe-NiO-12 on FTO substrate: (b) O; (c) Ni; (d) Fe. The homogenous distribution of Ni and Fe indicated a Fe-doped NiO rather than a segregated composite.

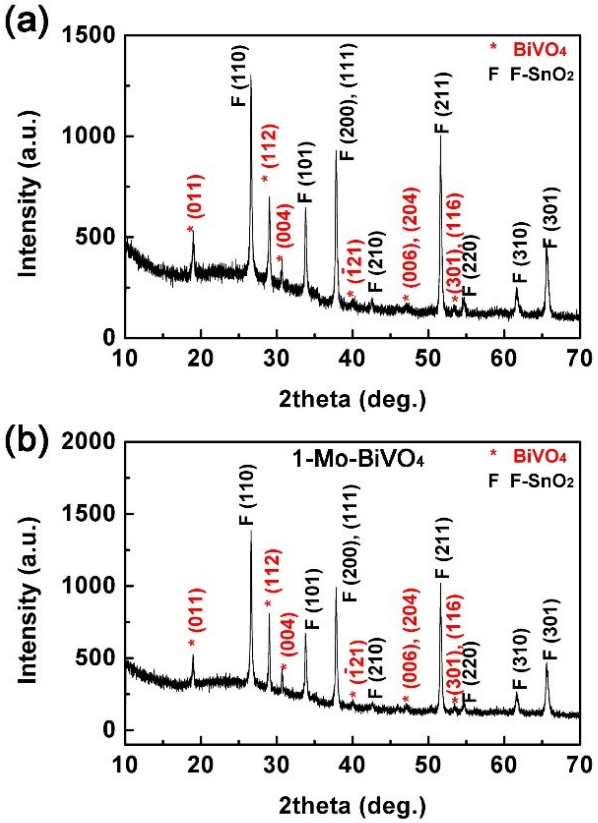

Figure S4. XRD of undoped $BiVO_4$: (a) and single step prepared 1-Mo-$BiVO_4$, (b) films on FTO substrate.

Table S1. Lattice parameters of the $BiVO_4$, 1-Mo-$BiVO_4$ and 2-Mo-$BiVO_4$.

	a (Å)	*b* (Å)	*c* (Å)	*γ*	*V*(Å^3)
$BiVO_4$	5.176	5.122	11.72	90.21°	310.71
1-Mo-$BiVO_4$	5.176	5.125	11.71	90.20°	310.63
2-Mo-$BiVO_4$	5.177	5.123	11.71	90.20°	310.57

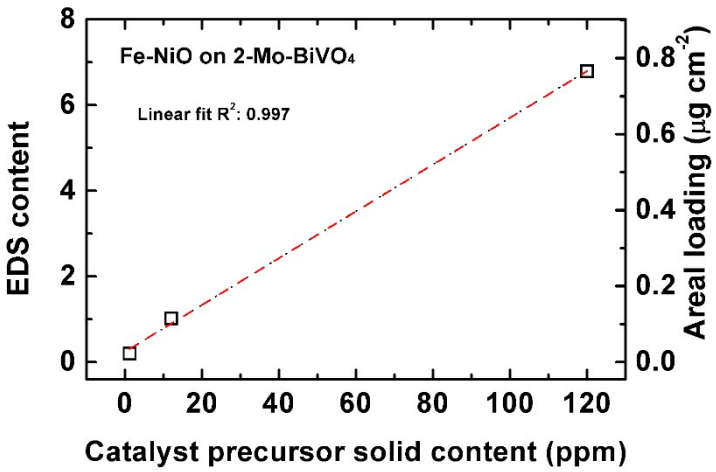

Figure S5. Fe-NiO catalyst loading amount on the 2-Mo-$BiVO_4$ films. The loading amount of Fe-NiO on the 2-Mo-$BiVO_4$ increased about 6.2 times for 10 times solid content increment of Fe-doped $Ni(OH)_2$ precursor.

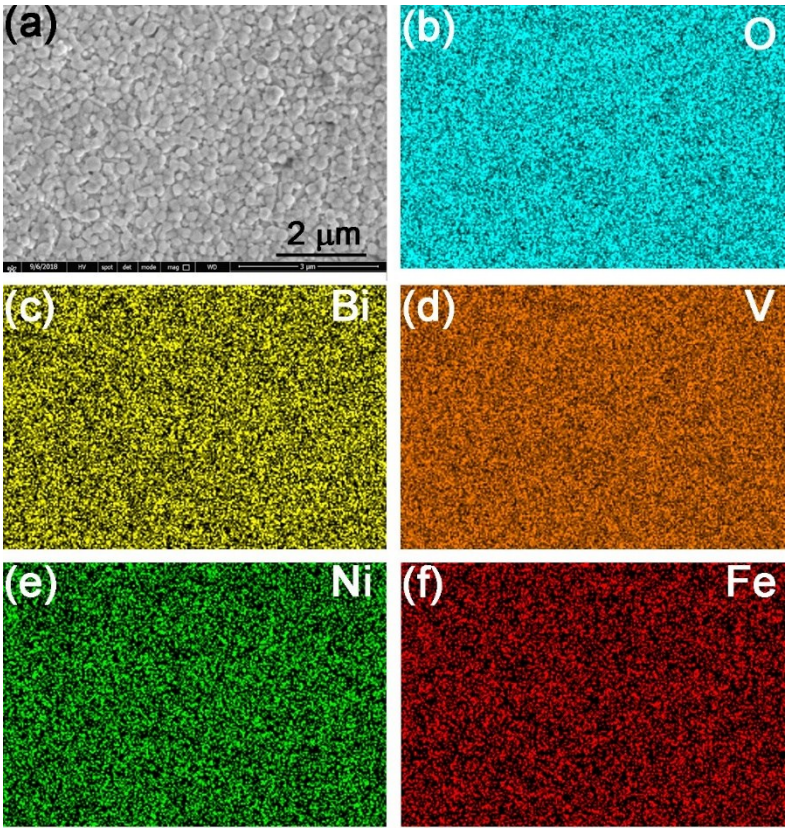

Figure S6. SEM image: (a) and EDS mapping image of the 2-Mo-$BiVO_4$/Fe-NiO-12 film: (b) O; (c) Bi; (d) V; (e) Ni; (f) Fe.

The EDS mapping of Ni and Fe showed homogenously distribution in the chosen region, indicating a well dispersion of the Fe-NiO electrocatalyst on the surface of the 2-Mo-$BiVO_4$ film.

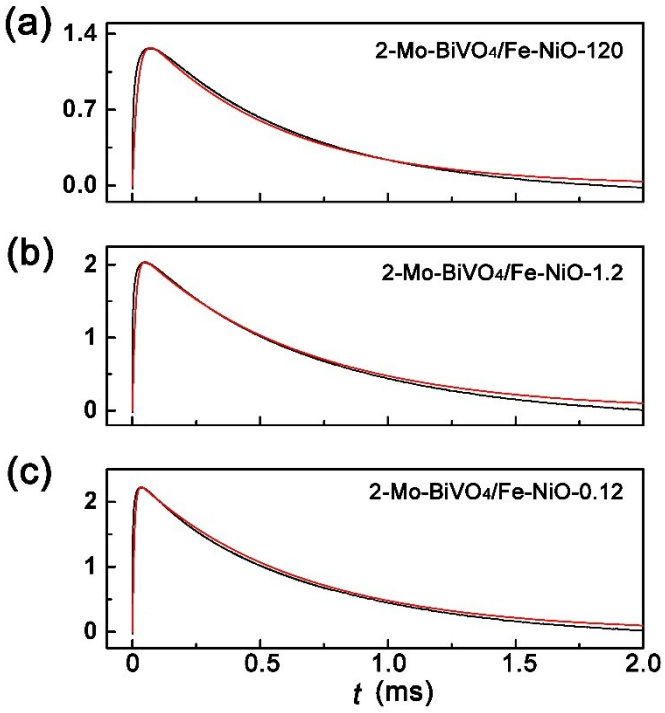

Figure S7. Experimental and simulation of TSPV curves for the 2-Mo-$BiVO_4$/OEC: from top to bottom are modified by (a) Fe-NiO-120, (b) Fe-NiO-1.2 and (c) Fe-NiO-0.12, respectively.

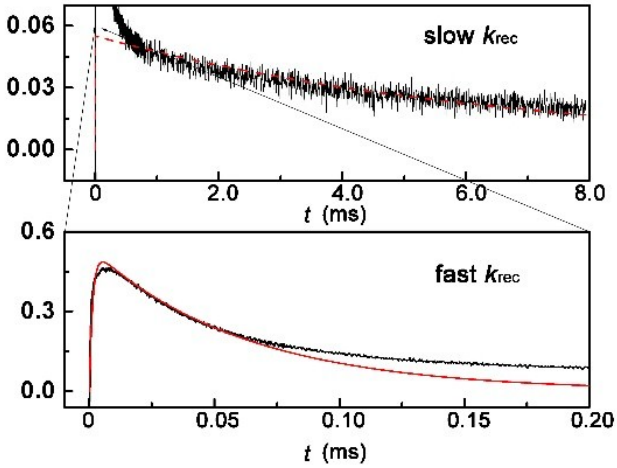

Figure S8. Experimental and simulation for the of TSPV curves 2-Mo-$BiVO_4$/$NiFeO_x$. The charge recombination showed a fast and a slow recombination processes, indicating the thick amorphous $NiFeO_x$ layer display a prolonged lifetime for the separated charge. The $NiFeO_x$ OEC films are prepared according the literature method (Smith R. D. L. et al., Science, 2013, 340, 60-63).

Table S2. Summary of charge separation and recombination kinetics with various catalysts.

Semiconductor films	t_{max} (s)	k_{sep} (s^{-1})	k_{rec} (s^{-1})	$Q_{exc,0}$ (a.u.)[b]	$Q_{sep,max}$
2-Mo-$BiVO_4$/Fe-NiO-120	7.1×10^{-5}	4.8×10^{4}	1.85×10^{3}	1.45	1.26
2-Mo-$BiVO_4$/Fe-NiO-1.2	4.9×10^{-5}	8.2×10^{4}	1.55×10^{3}	2.20	2.02
2-Mo-$BiVO_4$/Fe-NiO-0.12	3.4×10^{-5}	1.3×10^{5}	1.60×10^{3}	2.35	2.22
2-Mo-$BiVO_4$/a-$NiFeO_x$[a]	5.3×10^{-6}	7.3×10^{5}	1.64×10^{4}	0.53	0.48
	1.2×10^{-5}	7.3×10^{5}	1.50×10^{2}	0.055	0.055

a. back illumination for thick amorphous $NiFeO_x$ water oxidation catalyst.

b. the relative value of the $Q_{exc,0}$ were shown here (set C=1).

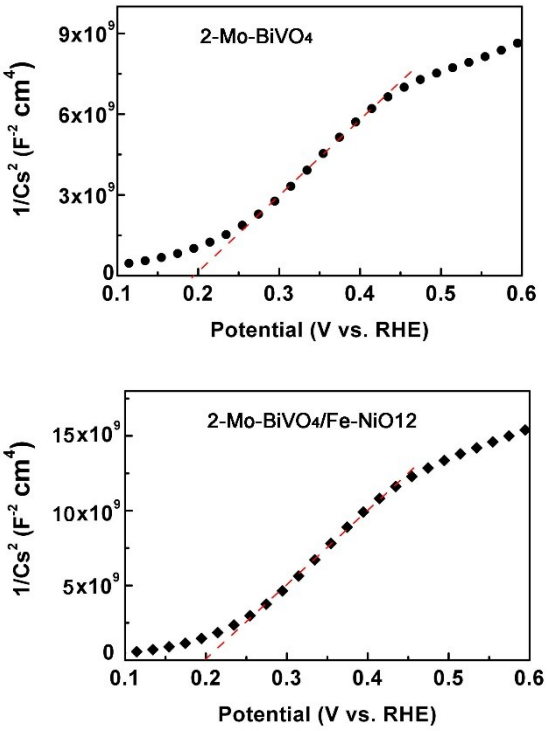

Figure S9. Mott-Schottky plots for the 2-Mo-$BiVO_4$ and 2-Mo-$BiVO_4$/Fe-NiO-12 films on FTO substrates respectively. The electrolyte was 1 M NaOH, containing 2 mM $[Fe(CN)_6]^{3-}$/$[Fe(CN)_6]^{4-}$. The electrodes were measured at 1 kHz, with potential amplitude of 5 mV.

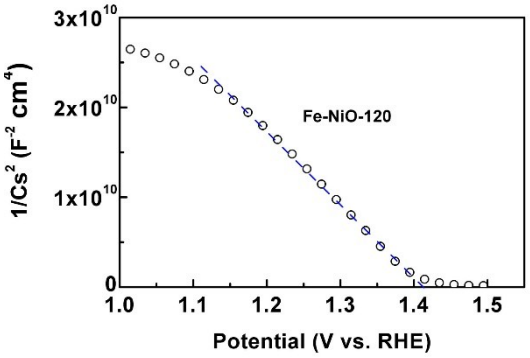

Figure S10. Mott-Schottky plot for the Fe-NiO-120 film on FTO substrates respectively. The electrolyte was 1 M NaOH, containing 2 mM $[Fe(CN)_6]^{3-}$/$[Fe(CN)_6]^{4-}$. The electrodes were measured at 1 kHz, with potential amplitude of 5 mV.

Table S3. The photoelectrochemical *J-V* performance of the bismuth vanadate photoanode in alkaline solution.

	Film structure	Electrolyte	Illumination	V_{on} V/RHE	*J*@1.4 V mA/cm^2	Reference
$BiVO_4$	Planar	1 M NaOH (pH13.5)	Back	0.55	0.12	This work
1-Mo-$BiVO_4$	Planar	1 M NaOH (pH13.5)	Back	0.27	0.4	This work
2-Mo-$BiVO_4$	Planar	1 M NaOH (pH13.5)	Back	0.27	0.88	This work
$BiVO_4$	-	0.1 M NaOH (pH12.7)	-	0.26	<0.03	1
$BiVO_4$	Planar	KOH (pH13)	Front	0.69	0.40	2
$BiVO_4$	Planar	0.1 M KOH (pH13), 1.35sun	-	0.64	0.66	3
$BiVO_4$	Nanoporous	1 M KOH	-	0.41	1.20	4
$BiVO_4$	Nanoporous	0.1 M KOH (pH13)	Back	0.48	1.28	5

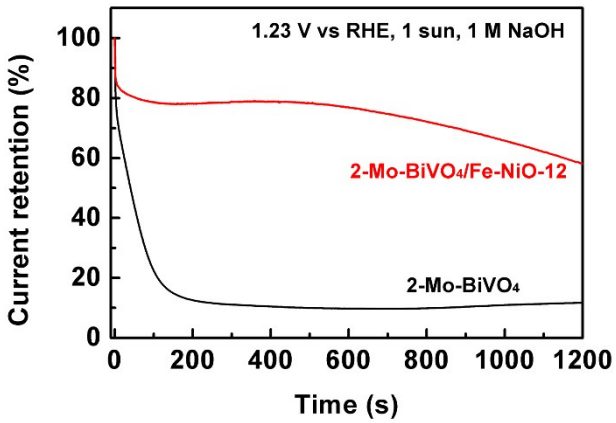

Figure S11. Photoelectrochemical stability of bare and Fe-NiO-12 modified 2-Mo-$BiVO_4$ photoanode. The measurement was carried out at 1.23 V vs. RHE under simulated solar light (AM 1.5G, 1 sun) in 1 M NaOH electrolyte.

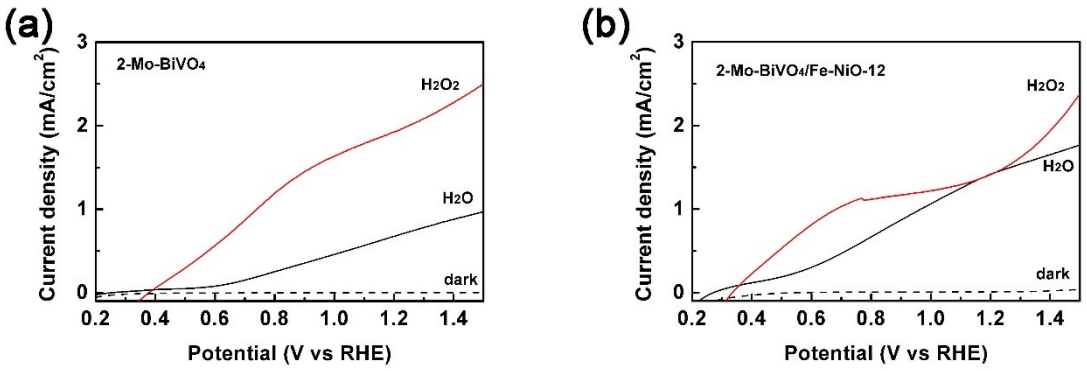

Figure S12. *J-V* curves in 1 M NaOH (with and without 100 μL H_2O_2): (a) bare 2-Mo-$BiVO_4$ and (b) 2-Mo-$BiVO_4$/Fe-NiO-12.

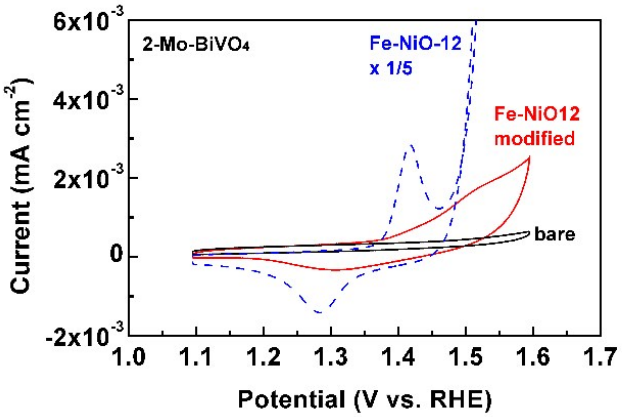

Figure S13. Cyclic voltammetry curves of the electrodes: red curve is the 2-Mo-$BiVO_4$ photoanode modified by Fe-NiO ultrathin nanosheets from 12 ppm dispersion; black curve is the bare 2-Mo-$BiVO_4$ photoanode; blue dashed curve is the Fe-NiO nanosheets on FTO substrate from 12 ppm dispersion, which current was divided by 5 for comparison. The measurement was conducted under 20 mV/s of the sweeping rate in 1 M NaOH electrolyte under dark condition.

From the Figure S13, the red curve clearly showed the increased current of the Fe-NiO modified 2-Mo-$BiVO_4$ in the potential window of 1.2-1.6 V vs. RHE. This phenomenon can further confirm the charge storage in the Fe-NiO ultrathin nanosheets.

Reference:

1. M. Long and W. Cai, *Chinese Journal of Catalysis*, 2008, **29**, 881-883.
2. M. F. Lichterman, M. R. Shaner, S. G. Handler, B. S. Brunschwig, H. B. Gray, N. S. Lewis and J. M. Spurgeon, *J. Phys. Chem. Lett.*, 2013, **4**, 4188-4191.
3. M. T. McDowell, M. F. Lichterman, J. M. Spurgeon, S. Hu, I. D. Sharp, B. S. Brunschwig and N. S. Lewis, *J. Phys. Chem. C*, 2014, **118**, 19618-19624.
4. B. Liu, H.-Q. Peng, C.-N. Ho, H. Xue, S. Wu, T.-W. Ng, C.-S. Lee and W. Zhang, *Small*, 2017, **13**, 1701875.
5. T. W. Kim and K.-S. Choi, *J. Phys. Chem. Lett.*, 2016, **7**, 447-451.